**Eur. Phys. J. C manuscript No.**
(will be inserted by the editor)

# First results of the OMC4DBD project on ordinary muon capture in $^{136}$Ba and $^{76}$Se

**D.Bajpai[1], V. Belov[2], L. Baudis[3], E. Bossio[4], T. Comellato[4], T.E. Cocolios[5], H. Ejiri[6], M. Fomina[2], I.H. Hashim[7], M. Heines[5], K. Gusev[2,4], L. Jokiniemi[8], S. Kazartsev[2,9], A. Knecht [10], E. Mondragon[4], Z.W. Ng[7], F. Othman[7], I. Ostrovskiy[b,1], G. Rodrigues Araujo[3], N. Rumyantseva[2], M. Schwarz[4], S. Schönert[4], M. Shirchenko[2], E. Shevchik[2], Yu. Shitov[2], S.M. Vogiatzi[10,12], C. Wiesinger[4,13], I. Zhitnikov[2], D. Zinatulina[a,2], MONUMENT collaboration**

[1] Department of Physics and Astronomy, University of Alabama, Tuscaloosa, AL, USA
[2]Joint Institute for Nuclear Research, Dubna, Russia
[3]Physik-Institut, University of Zurich, Zurich, Switzerland
[4]Technische Universität München, Garching, Germany
[5]KU Leuven, Institute for Nuclear and Radiation Physics, Leuven, Belgium
[6]Research Center on Nuclear Physics, Osaka University, Ibaraki, Osaka, Japan
[7]Department of Physics, Universiti Teknologi Malaysia, Johor Bahru, Malaysia
[8]Department of Quantum Physics and Astrophysics and Institute of Cosmos Sciences, University of Barcelona, Barcelona, Spain
[9]Voronezh State University, Voronezh, Russia
[10]Paul Scherrer Institut, Villigen, Switzerland
[11]Department of Physics, University of Jyväskylä, Jyväskylä, Finland
[12]ETH Zürich, Switzerland
[13]Max Plack Institute für Physik, Munich, Germany
Received: date / Accepted: date

**Abstract** The Ordinary Muon Capture for Double-Beta Decay project, or OMC4DBD, is aimed to measure the ordinary muon capture (OMC) in order to investigate neutrino nuclear responses for isotopes relevant for neutrinoless double-beta ($0\nu\beta\beta$) decay . The results of OMC measurements help improving $0\nu\beta\beta$ nuclear matrix element (NME) calculations and understanding of the $g_A$ quenching, thus advancing the physics of next-generation $0\nu\beta\beta$ searches. This work extends our previous program of OMC measurements to heavy $0\nu\beta\beta$ daughter nuclei, namely to $^{136}$Ba, $^{76}$Se and $^{96}$Mo. We present the first results obtained during the 2021 measurement campaign at PSI, including the absolute muon lifetime and the relative strength distribution for the three isotopes. –More specifics about the results– . These results will help improving $0\nu\beta\beta$ shell model calculations in the heavy mass region.

**Keywords** neutrino properties · ordinary muon capture reactions · total and partial muon capture rates · neutrinoless double-$\beta$ decay · nuclear structure · $\mu$X- and $\gamma$-ray spectroscopy · nuclear matrix elements

**PACS** 23.40.-s $\beta$ decay; double-$\beta$ decay; electron and muon capture · 29.30.Kv X- and $\gamma$-ray spectroscopy

[a]e-mail: zinatulina@jinr.ru
[b]e-mail: iostrovskiy@ua.edu

## 1 Introduction

Neutrino nuclear responses are crucial for neutrino studies in nuclei. Neutrino properties, such as the Majorana nature and the absolute mass scale, can be studied by neutrinoless double-beta ($0\nu\beta\beta$) decay [1–5, 7]. This process is typically represented as a two-stage transition including the parent, intermediate and daughter nuclei, with the $\beta^-$ and $\beta^+$ responses as its two branches. Their detailed studies are necessary in order to access quantitatively the neutrino properties beyond the standard model using the $0\nu\beta\beta$ experimental data. The nuclear matrix element (NME) of $0\nu\beta\beta$ decay, $M_{0\nu}$, is expressed in terms of the product of $\beta^-$ and $\beta^+$ matrix elements ($M(\beta^-)$ and $M(\beta^+)$) via the neutrino potential [6].

The search for $0\nu\beta\beta$ decay has recently been recognized as a top priority in particle and astroparticle physics by the AstroParticle Physics European Consortium (APPEC), which recommends a dedicated experi-

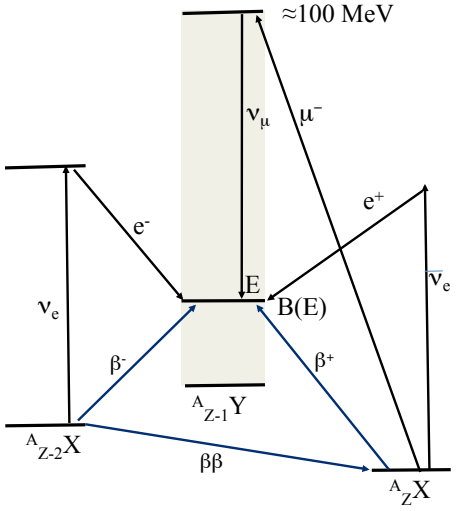


Fig. 1: $0\nu\beta\beta$ and muon charge exchange reaction schemes.

mental effort, in collaboration with the nuclear physics community, to improve the determination of NMEs [11].

An open problem in translating the half-life (rate) of $0\nu\beta\beta$ decay into the absolute neutrino mass scale is the potential quenching of the axial-vector coupling constant, $g_A$, in this process [19–21]. While it is established that strong quenching is needed to reproduce the rates of many $\beta$ and $2\nu\beta\beta$ decays, one cannot directly compare them to the $0\nu\beta\beta$ decay due to the much larger momentum transfer occurring during the latter process. Serendipitously, a similar momentum transfer occurs during ordinary muon capture (OMC) process, making it an attractive tool to experimentally study this topic.

OMC (see Fig. 1) is a charge exchange reaction mediated by a W boson. It involves the capture of a negative muon by a proton in a target nucleus, resulting in production of a neutron and a muon neutrino. The response represents the square of the nuclear matrix element, $M(\mu)$, which is equivalent to the $M(\beta^+)$ side of the $M_{0\nu}$ [33, 34]. The unique feature of OMC is the large energy and momentum transfers, on the order of $E$=0-50 MeV and $p$= 20-100 MeV/c, which are similar to the ones involved in $0\nu\beta\beta$ decays and medium-energy supernova neutrinos. The negative muons are first trapped in an atomic orbit and cascade down to the muon K-shell. Simultaneously with the muon stop, muonic X-rays are emitted. After that, there are two paths for the muon, which is either capture by the nucleus or decay to an electron and two neutrinos. In the first case, prompt $\gamma$-rays can be emitted. In the second case, a high-energy electron (Michel electron) is emitted.

In OMC, a well-bound proton in the target nucleus ${}^{A}_{Z}X$ is shifted up to a vacant neutron shell, which results mostly in the excitation of the nucleus ${}^{A}_{Z-1}\mathrm{Y}^{*}$ with the excitation energy $E$. If the excited nucleus is in a bound state, it decays by emitting $\gamma$-rays to the ground state ${}^{A}_{Z-1}\mathrm{Y}$. On the other hand, if ${}^{A}_{Z-1}\mathrm{Y}^{*}$ is unbound, it de-excites by emitting a number ($x$) of neutrons. In the case of medium-heavy nuclei, proton emission is mostly suppressed by the Coulomb barrier. Finally, the residual nucleus ${}^{A-x}_{Z-1}Y$ is obtained. If it is radioactive, we identify it by measuring characteristic $\gamma$-rays of the residual nucleus. The number of the emitted neutrons reflects the excitation energy $E$, with larger $x$ corresponding to a higher $E$ region.

The OMC reaction $A(\mu,\nu)$ normally is an order of magnitude less intense than a similar one followed by the emission of one or more neutrons. As a result, even a small contamination of the target with heavier isotopes (A+1) or (A+2) could lead to a parasitic population of the same excited states of the daughter nucleus. Therefore, from the experimental point of view, it is very important to use isotopically enriched targets without a significant content of the (A+1) or (A+2) isotopes.

Previously, we studied OMC on several isotopes relevant for $0\nu\beta\beta$ decay. Among them are $^{48}$Ti, $^{150}$Sm, $^{76}$Se, $^{106}$Cd, $^{82}$Kr [45]. In this work, we continue the measurement program by studying OMC on $^{136}$Ba, $^{76}$Se.

The description of the used set-up, detectors, their holder frame, muon veto trigger system are presented in Sections 2.2. Two data acquisition (DAQ) systems, called LLAMA and MIDAS, used in parallel, have been incorporated into the setup (see Section 3).

In October 2021, we had a beam time for four weeks. The first week of the experimental campaign was dedicated to mounting of the setup and tuning of the beam. The energy calibration of the detector array was performed during a beam-off period in the second week, followed by the measurements with isotopically enriched $^{136}BaCO_3$ and $^{76}$Se. More details are provided in Section 2.1.

Time and energy gamma spectra have been constructed and analysed. The total muon capture rates for the measured isotopes have been extracted. The results for $^{136}$Ba and $^{76}$Se are shown is Section 6.

## 2 Measurement principle

The idea of $\mu$-capture experiments is based on a precise measurement of the time and energy distributions of the $\gamma$-rays following the $\mu$-capture. These distributions provide rich experimental information, all of which serves as a useful input to the $\beta\beta$ NME calculation. The total

muon capture rates of specific isotopes are extracted by analyzing the time distribution of delayed $\gamma$-rays. The measured intensities of the delayed $\gamma$-rays give partial muon capture rates to the bound states. The yields of the short-lived isotopes are obtained using the beam-off and off-line measurements. An important by-product of the measurements is the $\mu$X-rays data. It helps to identify the type of atoms by which the muons were captured and serves as a normalization for the total number of stopped muons.

### 2.1 Targets

As was mentioned above, isotopically enriched targets are strongly preferable. On the other hand, measurements with the natural targets are also important for comparison and identification of numerous $\gamma$-lines in all measured spectra. Table 1 lists the targets which we used to investigate in this study.

Two grams of elemental selenium in powder form were press formed by applying 20 MPa of pressure. The resulting tablet has dimensions of 20 mm in diameter and 1.8 mm thickness.

Table 1: List of targets used in the present $\mu$-capture experiment in 2021. In the fourth column the element mass of the target itself is given.

| target | enr-ment | composition | element |
|---|---|---|---|
| $^{136}$Ba | 95.27% | $BaCO_3$ powder | 2.0 g |
| $^{nat}$Ba | – | $BaCO_3$ powder | 2.0 g |
| $^{76}$Se | 99.68% | Se elemental | 2.0 g |
| $^{nat}$Se | – | Se elemental | 2.0 g |

The natural-abundance and enriched barium targets were made using $^{nat}BaCO_3$ and $^{136}BaCO_3$ salts in powder form. After several attempts to develop a suitable technology, we settled on a process of depositing a solution of barium carbonate in isopropanol onto a plastic holder and allowing it to dry before closing the holder securely with a lid.

### 2.2 Description of the setup

The target unit, sketched in Fig 2, consists of an active muon veto counter, C0, placed at the entrance of the target enclosure, two thin (0.5 mm) pass-through counters, C1 and C2, and the actual target area surrounded by a cup-like counter, C3.

The C3 counter together with the pass-through counters are used to define a $\mu$-stop trigger:

$$\mu_{stop} = \overline{\mathrm{C0}} \wedge \mathrm{C1} \wedge \mathrm{C2} \wedge \overline{\mathrm{C3}} \quad (1)$$

as well as to discriminate high-energy electrons coming from the muon decays. Since it is made from a low-Z material, C3 does not affect the measurements of low energy (20-100 keV) $\gamma$-rays by the external germanium detectors.

The beam momentum and position were tuned to maximize the intensity of $\mu$X-rays from the target and minimize the background from the surrounding material. Under optimal conditions, more than 95% of the collected data should correspond to muons stopped in the target. Typical $\mu_{stop}$ rates during the experiment were between $10^4$ $s^{-1}$ and $4{\times}10^4$ $s^{-1}$.

Fig. 3 shows the setup used in the 2021 measurement campaign. The set consists of a total of nine HPGe detectors. Eight of them are placed around the target, while the ninth is a standalone detector placed under the setup in order to monitor the background. The eight detectors surrounding the target are of the following three types:

1. Four large-volume n-type coaxial detectors (**REGe** detectors) with thin beryllium entrance windows.
2. Two large-volume p-type coaxial detectors (**COAX** detectors).
3. Two relatively large-volume p-type **BEGe** detectors with thin beryllium entrance windows.

The eight main detectors are mounted to an aluminum frame at a distance of about 15 cm from the target. The frame is made of a standard industrial 40x40 mm aluminum profile that allows one to adjust the position of the detectors around the target.

## 3 Data acquisition system

During our measurements in 2021 campaign two independent DAQ systems have been used. One based on the muX experiment, which is belong to PSI (described in 3.1), and second new DAQ system has been incorporated in parallel with the MIDAS (see 3.2). Here we present the results from the data taken with the MIDAS DAQ system. The analysis from the LLama DAQ is in progress.

### 3.1 MIDAS DAQ

The DAQ system and software from the muX experiment have been used during the 2021 $\mu$-capture measurements to collect and analyze the data, specifically

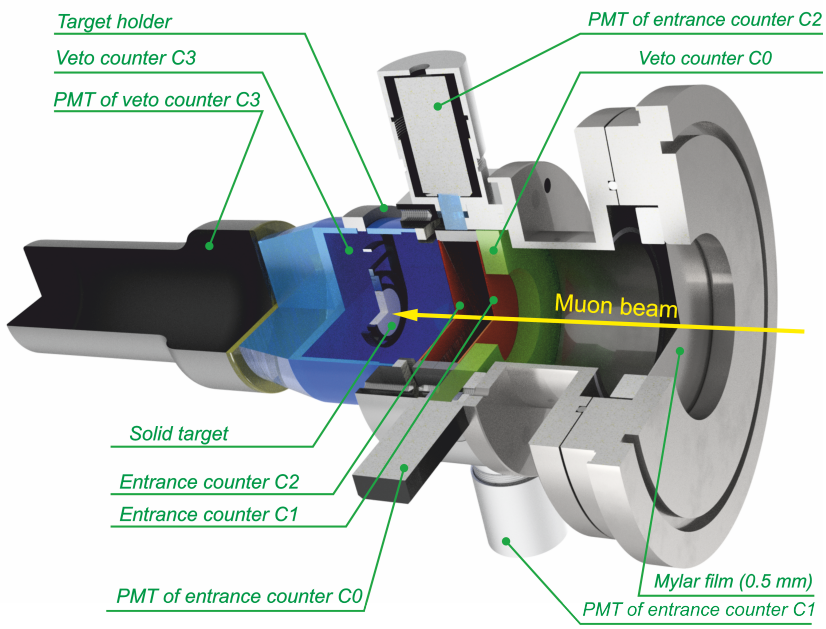


Fig. 2: Picture of the solid target unit with the scintillation counters

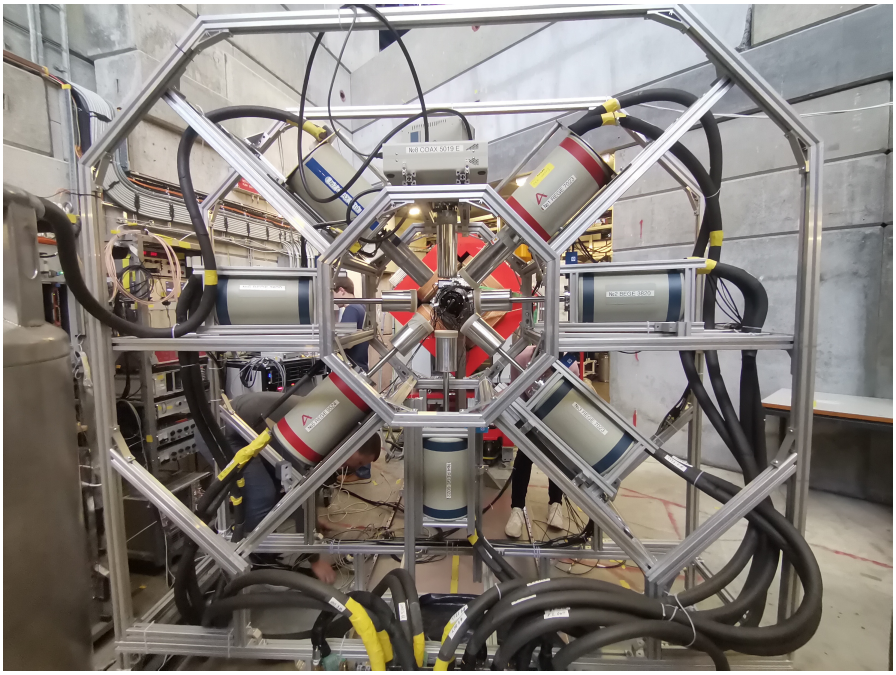

Fig. 3: Picture of the setup showing the germanium detector array mounted around the target at the end of the $\pi$E1 beamline.

the energy and time of incoming events (muons and gammas).

The DAQ system is based on a Struck SIS3316 digitizer module [24] with 16 channels, 14-bit resolution, sampling rate of 250 MHz, and a selectable input range of 2 to 5 V. The firmware of the FPGAs allow one to use the trapezoidal filtering during the pulse height analysis of the HPGe signals. The operation and settings of the module are fully integrated into the MIDAS acquisition system [25], which provides for a robust and reliable tuning and data taking.

### 3.2 LLAMA DAQ system for OMC4DBD

This text should be corrected/ written by TUM group

## 4 Online data taking

The online data taking was started with $^{nat}$Ba. During this measurement, the beam tuning and energy and efficiency calibrations were performed. The beam momentum was tuned to maximize the stopping of muons exactly in the target. $^{136}$Ba was measured after $^{nat}$Ba for 96 hours. Since both the natural and enriched barium targets have the same composition, the beam tuning did not need to be repeated. $^{136}$Ba was then moved to the offline measurements and replaced with $^{76}$Se. The two grams of isotopically enriched $^{76}$Se were measured for 105 hours. The data analysis is described below.

### 4.1 Data acquired with MIDAS DAQ

The MIDAS DAQ data were converted for further analysis to ROOT trees. Each event contains non-calibrated energy, timestamp (improved offline for the HPGe detectors), precalibrated energy (only for the HPGe detectors), detector ID and technical information about overflows, underflows, and pileups during pulse digitization by the Struck FADC.

A simple way to identify muons stopped in the target is to require a coincidence within the 100 ns window between the C1 and C2 counters, C1 $\wedge$ C2. To remove muons that miss the target and get captured by the surrounding materials, the $\overline{\text{C0}}$ condition 1440 ns before the C1 $\wedge$ C2 is used. The latter time window is driven by the dead time of the digitizer.

The two conditions are used as a "soft" muon trigger. Further improvement is achieved by requiring both $\overline{\text{C0}}$ and $\overline{\text{C3}}$ during 1440 ns before the C1 $\wedge$ C2. This "hard" muon trigger may additionally remove some of the background from high-energy electrons associated with muons decays. Fig. 4 shows the statistics of triggers by the individual scintillator counters of the target unit, as well as the (anti)coincidences between them.

### 4.2 Data acquired with LLAMA DAQ

This text should be corrected/written by TUM group

## 5 Data analysis methods

The experimental procedures used in this work are discussed in detail separately in the following subsections.

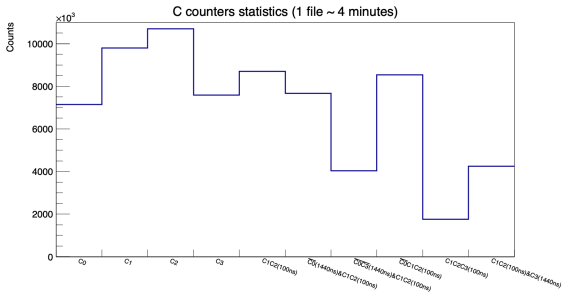


Fig. 4: Events statistics from C counters and some coincidences between them (MIDAS DAQ).

### 5.1 Spectra reconstruction and $\gamma$-line identification

The first step in data processing is the reconstruction of gamma spectra of various types and the identification of $\gamma$-lines to assess the experimental conditions and statistics accumulated. HPGe detector events are selected by special conditions relating to the hard software trigger with the 1440 ns time window, which was described earlier. The selected events are sorted into the following distinct types:

1. HPGe events occurring during the time window following the main trigger (and no other trigger from any of the C counters) form the **Correlated** spectra.
   (a) HPGe events occurring in the first 100 ns from the main trigger form the **Prompt** spectrum.
   (b) Events within the time window that occur later than 100 ns since the main trigger form the **Delayed** spectrum.
2. HPGe events with the main trigger and an additional trigger from any of the C counters during the selected time window form the **Rejected** spectra.
3. HPGe events occurring outside of the selected time window opened by a trigger in any of the C counters form the **Uncorrelated** spectra.
4. HPGe events not subject to any of the conditions form the **All** spectra.

The sum of the **Prompt** and **Delayed** spectra is equal to the **Correlated** spectrum, while the sum of the **Correlated**, **Uncorrelated**, and **Rejected** spectra is the **All** spectrum. As an example, such spectra for $^{76}$Se are presented in Fig. 5.

Events from the HPGe detectors collected during the online measurements can be divided into two types – events correlated and uncorrelated in time with the incoming muons. If an event from the HPGe detectors is not preceded within some time window by a muon that stopped in the target, then the event is considered

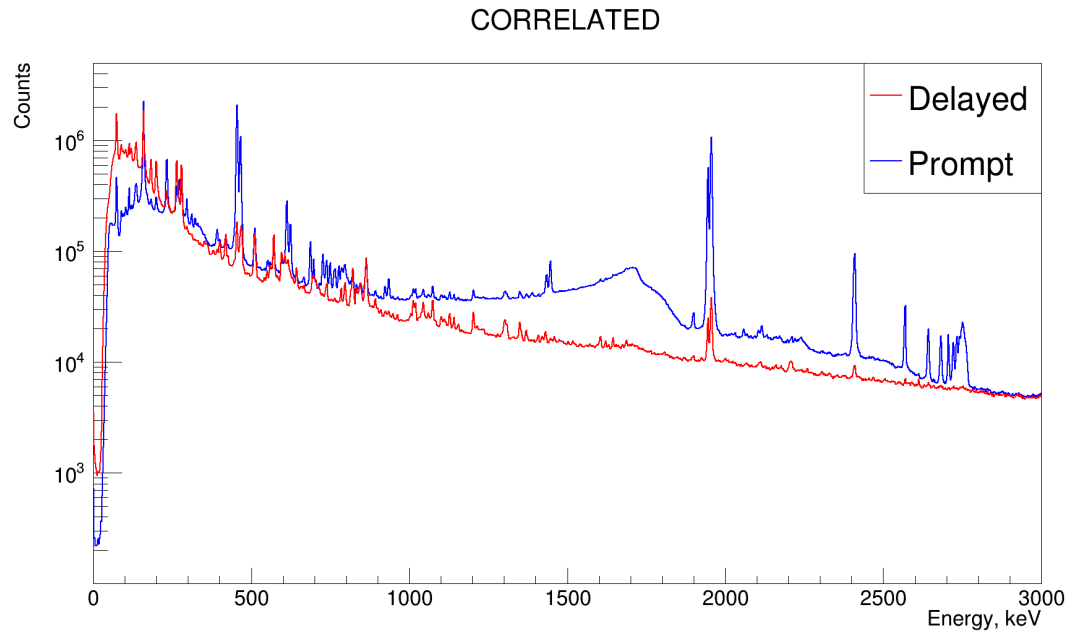


(a)

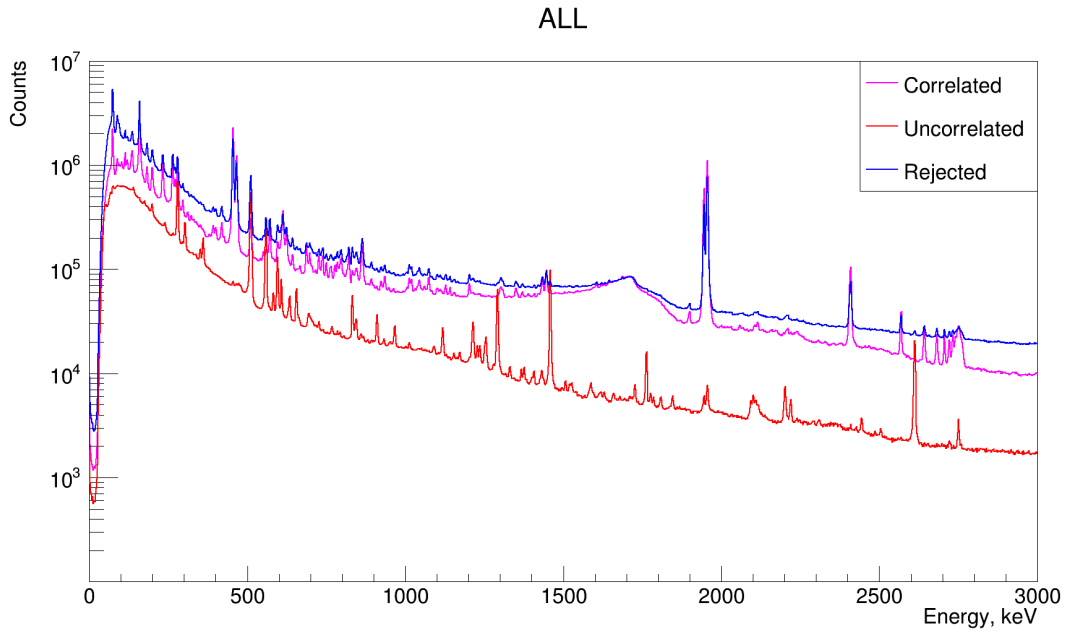


(b)

Fig. 5: (a) – $^{76}$Se spectra for correlated events (detector #2); (b) – $^{76}$Se spectra for all events (detector #2).

uncorrelated. A typical **Uncorrelated** spectrum includes $\gamma$-lines from natural ($^{40}$K, U, and Th chains) and man-made ($^{60}$Co, $^{137}$Cs) backgrounds, as well as beam-induced $(n, \gamma)$-reactions. These lines could be used to calibrate the detectors.

Correlated events are those that occur within the time window immediately after the $\mu$-stop. They are more informative. Mostly of such events are caused by a cascade of the muonic X-rays ($\mu$X) – high energy photons emitted by a muonic atom during its transition to the 1s state from a Rydberg stage. The de-excitation process takes place within picoseconds, so that $\mu$X-ray can be considered a prompt radiation.

In addition to these prompt events, delayed correlated events correspond to the nuclear $\gamma$ radiation fol-

lowing muon capture in the $(\mu^-, \nu\ xn)$ reactions. This particular radiation is the main subject of our work.

The relative intensity of the delayed lines (with respect to the $\mu$X-rays) allows one to extract the partial capture rates to the individual excited states of the daughter nucleus. In order to simplify the $\gamma$-line identification, the **Prompt** and **Delayed** spectra shown in Fig. 5(a) are partially separated from each other by a time cut.

The muon lifetime in a muonic atom of the target under study is determined by the competition of two processes: i) muon decay with emission of a muon neutrino and a Michel electron, ii) muon capture by a proton of the target nucleus with emission of a muon neutrino.

Both processes can be used to determine the muon lifetime on the atoms of the target under study, and both processes are actually used by us to determine the muon lifetime by two independent methods, discussed in detail below.

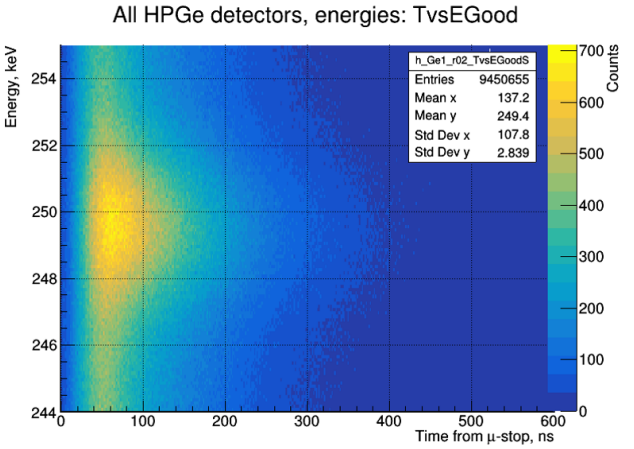


Fig. 6: Part of the (E,t) distribution around $^{135}$Cs 249.7 keV line measured with the $^{136}$Ba target.

An example of fitting the $^{136}$Ba 250 keV line is shown in Fig. 8

### 5.2 Determination of the muon lifetime from the OMC

In the process of OMC, the energy of $100 MeV$ is transferred to the reaction products, which leads to the formation of excited daughter nuclei that emit characteristic $\gamma$-lines during de-excitation. Measuring the exponential time evolution of these $\gamma$-lines makes it possible to determine the OMC probability by a dedicated method described in [27, 45].

At the first step of data processing, we obtain two-dimensional (E,t)-spectra of the studied characteristic $\gamma$-lines (see Fig. 6). The subsequent analysis consists of the following steps (see Fig. 7).

A) Construction of a 1D-energy spectrum by the projection of a 2D-histogram onto the energy axis and its fitting with the Gauss plus a linear background model. The obtained peak position $E_0$ and its resolution $(\sigma)$ are used as fixed parameters in further fits.

B) Construction of a successive series of energy slices along the time axis, each of which is fitted by the Gauss + linear background model at fixed position and resolution parameters obtained in step A). The output is the dependence of the intensity of the $\gamma$-line on time after OMC.

C) Fitting the obtained dependence with an exponential function $f = A * exp(-\lambda * t) + C$, where the $\lambda$ is the parameter of interest.

Carrying out this analysis for a number of the strongest characteristic gamma lines of the target under study allows a precise determination of the muon lifetime in the isotope under study.

### 5.3 Determination of the muon lifetime from muon decay

The concept of the proposed methodology is shown in Fig. 9. The muon passes through the system of counters and stops in the target under study ($\mu$-stop is determined by $\bar{C}0\&C1\&C2\&\bar{C}3$ trigger logic). After the formation of a muonic atom (the formation time of which can be considered instantaneous for our case), a part of the muons decays with the emission of a muon neutrino and a Michel electron, registered by the C3 counter.

This method is described in [40] and was used to determine the muon lifetime in various substances at the early stage of the mu-capture physics. The main problem in this technique is the possibility of stopping and decaying muons not in the target material, but outside it (counters, air, etc.). Since the muon lifetime in materials outside the target can differ greatly from the muon lifetime in the material under study, this introduces a significant systematic error, which is difficult to control.

In order to get rid of this problem, in our experiment, we have the opportunity to impose an additional cut - the coincidence of the $\mu$-stop in the target region with the registration of the characteristic $\mu$X-ray in a HPGe corresponded to the studied isotope $(\bar{C}0\&C1\&C2\&HPGe(\mu X)\&\bar{C}3$ trigger logic).

One should emphasize that the coincidence of the $\mu$-stop with the characteristic muon X-ray of an element makes it possible to isolate the formation of the muonic atom of that particular element and to register a Michel

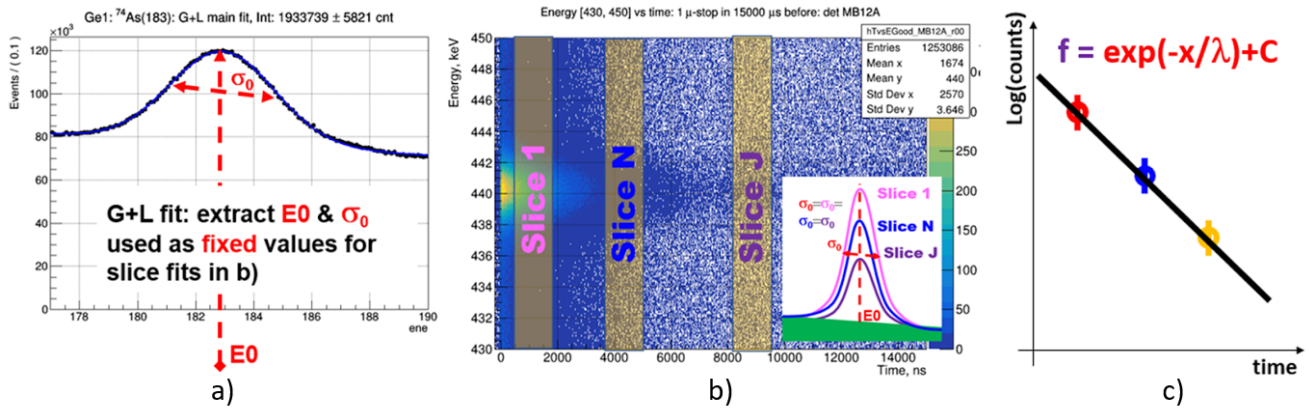


Fig. 7: Determination of the muon lifetime by the OMC method: a) fitting of the $\gamma$-line in the total energy spectrum, b) slicing along the time axis and fitting, c) fitting of the exponential attenuation in time of the $\gamma$-line under study.

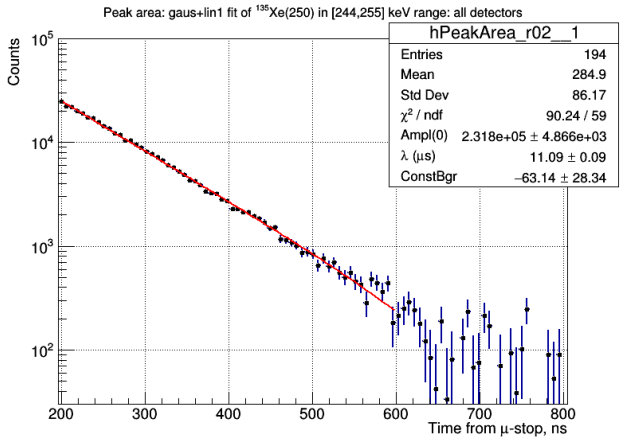


Fig. 8: Final stage fit of the $^{136}$Ba 250 keV line in the OMC method.

electron from the decay of a muon from this muonic atom.

This makes it possible to obtain and fit a pure (in terms of isolating a particular muon decay process under study) time spectrum of Michel electrons, an example of which is shown in Fig. 10.

## 6 Results and discussion

### 6.1 Muon lifetime in $^{136}$Ba

***The OMC approach.*** By investigating the intensities of the strongest $\gamma$-lines of $^{135}$Cs and $^{136}$Cs emitted after the OMC in $^{136}$Ba we extract the value of the muon lifetime in $^{136}$Ba:

$$\lambda_{\rm tot} = 86.2(55)\,\mu{\rm s}^{-1}(68\%CL) \quad (2)$$

***The muon decay approach*** We have obtained a value:

$$\lambda_{\rm tot} = 90.0(65)\,\mu{\rm s}^{-1}(68\%CL), \quad (3)$$

which is consistent with the one (2) obtained earlier from the OMC.

Thus, the two independent approaches give the same results within errors, which indicates the robustness of the estimate obtained.

### 6.2 Muon lifetime in $^{76}$Se

text will be applied later

### 6.3 Muon lifetime in natural barium

text will be applied later

### 6.4 Muon lifetime in natural selenium

text will be applied later

## 7 Summary

The presented experiment unravels the gross features of weak responses ($\beta^+$ strength distributions) with $J^\pi = 0^\pm, 1^\pm, 2^\pm, ...$ and $p$=30–100 MeV/c in $E$ = 0-70 MeV

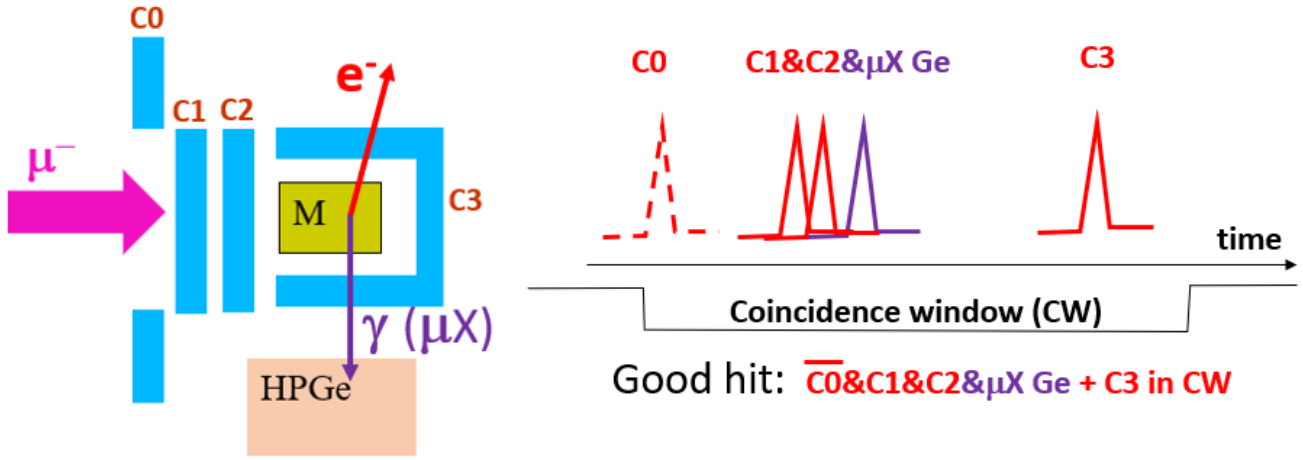


Fig. 9: Determination of the muon lifetime by the muon decay method: scheme (figure on the left) and logic of the searched event.

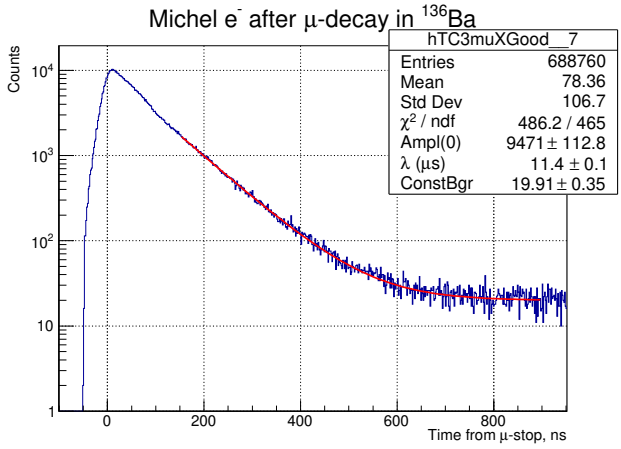


Fig. 10: Time distribution of Michel electrons from muon decay in a muonic $^{136}Ba$-atom (blue curve) and its exponential fit (red curve) with the results presented in the legend.

for isotopes of $^{136}$Ba and $^{76}$Se, which is the daughters nuclei of the DBD nuclei of $^{136}$Xe and $^{76}$Ge, respectively. It is used to get and/or evaluate the $0\nu\beta\beta$ responses ($|M_{0\nu}|^2$) and astro-$\nu$ responses for medium heavy nuclei.

As a result of that work the total $\mu$-capture rates in $^{136}$Ba and $^{76}$Se have been determined. For the $^{136}$Ba it was made first time, for the $^{76}$Se it was corrected and made with the 99,97% of the enrichment of $^{76}$Se. The future extraction of the partial $\mu$-capture probabilities (rates) to the bound states in $^{136}$Cs and $^{76}$As will be based on these results. Related to this, important information about the weak coupling constants and nuclear-theory aspects will be obtained from the muon-capture strength function and the associated giant resonance [43] when compared with the presently available [44] and future calculations of the strength functions. In this way the partial $\mu$-capture rates results will be an important contribution to a more accurate theoretical evaluations of the $0\nu\beta\beta$ NMEs.

**Acknowledgements** The OMC4DBD experiment is supported financially by the Joint Institute for Nuclear Research, and Max Plack Institute für Physik. This project has received funding/support from the Russian Foundation for Basic Research grant №, as well as from the German Research Foundation (DFG) №. This work was supported also by the the Swiss National Science Foundation (SNF). The cost of $^{136}$Ba are covered by a US Department of Energy Grant No. DE-SC0019261. The institutions acknowledge also internal financial support. The OMC4DBD collaboration thanks the directors and the staff of PSI for their continuous strong support of the OMC4DBD experiment.

## References

1. H. Ejiri, Phys. Rep. C 338 265 (2000) and refs. therein
2. H. Ejiri, Czechoslovak J Phys. 56 (2006) 459
3. H. Ejiri, Progress Particle Nuclear Physics 64 (2010) 249
4. H. Ejiri, J. Phys. Soc. Jap. 74 (2005)
5. J. Vergados, H. Ejiri, and F. Simkovic, Report Progress Physics 75 (2012) 106301
6. H. Ejiri, J. Suhonen, and K. Zuber, Phys. Rep. 797 (2019) 1

7. J. Suhonen and O. Civitarese Phys. Rep. 300 (1998) 123
8. H. Ejiri, Proc. EM interactions, Sendai. (1972)
9. I.H.Hashim, H.Ejiri et al. Phys. Rev. C 97 (2018) 014617
10. D.F. Measday, Physics Reports 354, 243 (2001)
11. A. Giuliani et al., arXiv:1910.04688 [hep-ex]
12. https://science.osti.gov/np/nsac
13. I. Ostrovskiy and K. O'Sullivan, Modern Physics Letters A, 31 (2016) 18, 1630017
14. nEXO Collaboration, arXiv:1805.11142v2 [physics.ins-det]
15. LEGEND @ APPEC-2019,
16. J.J. Gomez-Cadenas et al. Adv. High Energy Phys., 2014:907067
17. DARWIN Collaboration JCAP 1611 (2016) no.11, 017
18. S.M. Bilenky and C. Giunti International Journal of Modern Physics A 30 (2015) 1530001
19. J.T. Suhonen, Front. Phys. 5 (2017) 55
20. J. Suhonen Phys. Rev. C 96 (2017) 055501
21. J. Suhonen and J. Kostensalo, Front. Phys. 7 (2019) 29
22. P. Bergem et al., "Nuclear polarization and charge moments of $^{208}$Pb from muonic x rays",Phys. Rev. C **3**7 (1988) 2821
23. F.J. Hartmann, R. Bergmann, H. Daniel et al., "Measurement of the Muonic X-Ray Cascade in Mg, Al, In, Ho, and Au", Atoms and Nuclei **3**05 (1982) 189-204
24. http://www.struck.de/sis3316.html
25. http://midas.psi.ch.
26. L. Mihailescu, C. Borcea, A. Plompen, "Data acquisition with a fast digitizer for large volume HPGe detectors" Nucl. Instrum. Meth. A **5**78 (2007) 298
27. V. Egorov et al., Czech. J. Phys. **5**6 (2006) 453
28. D. Measday, "The nuclear physics of muon capture", Phys. Rep. **3**54 (2001) 243
29. R. Pehl et al., "Radiation Damage Resistance of Reverse Electrode Ge Coaxial Detector", IEEE T. Nucl. Sci. **2**6 (1979) 321
30. H. Ejiri et al., Phys. Rev. Lett. **8**5 (2000) 2917
31. I.H. Hashim. PhD thesis Osaka University (2014)
32. I.H. Hashim, H. Ejiri et al. Proposal for WSS-MuSIC beamtime. Osaka University (2016)
33. M. Kortelainen and J. Suhonen Europhys.Lett. **5**8 (2002) 666-672
34. M. Kortelainen and J. Suhonen Nucl.Phys. A **7**13 (2003) 501-521
35. D. Zinatulina et al., AIP Conference Proceedings **9**42, (2007) 91
36. C. Briancon et. al , Mesoroentgen Spectra Catalogue, Retrieved from http://muxrays.jinr.ru/
37. D. Zinatulina et. al, arXiv:1801.06969 [nucl-ex]
38. I.H. Hashim, H. Ejiri et. al., Proposal for WSS-MuSIC beamtime. Osaka University (2018)
39. V. Egorov et al., Experiment R-02-02, PSI.
40. D.F. Measday, Phys. Rep. **3**54 (2001) 243
41. National Nuclear Data Center and Brookhaven National Laboratory, Retrieved from http://www.nndc.bnl.gov
42. J.H. Thies et al., Phys. Rev. C **8**6 (2012) 014304
43. L. Jokiniemi, J. Suhonen, H. Ejiri, and I.H. Hashim, Phys. Lett. B **7**94 (2019) 143
44. L. Jokiniemi, J. Suhonen, Phys. Rev. C **1**00 (2019) 014619
45. D. Zinatulina et al., "Ordinary muon capture studies for the matrix elements in $\beta\beta$ decay", Phys. Rev. C **9**9 (2019) 024327
46. N. Abgrall et al., AIP Conference Proceedings **1**894 (2017) 020027